Ambient-pressure CVD of graphene on low-index Ni surfaces using methane: A combined experimental and first-principles study

Daniela L. Mafra, Jimena A. Olmos-Asar, Fabio R. Negreiros, Alfonso Reina, Ki Kang Kim, Mildred S. Dresselhaus, Jing Kong, Gary J. Mankey, and Paulo T. Araujo

Ambient pressure CVD of graphene on low-index Ni surfaces using methane: a combined experimental and first-principle study

Daniela L. Mafra[1], Jimena A. Olmos-Asar[2,3,*], Fabio R. Negreiros[2,3,*], Alfonso Reina[4], Ki Kang Kim[5], Mildred S. Dresselhaus[1,6], Jing Kong[1], Gary J. Mankey[7,8] and Paulo T. Araujo[7,8,9,*]

[1]Department of Electrical Engineering and Computer Sciences, Massachusetts Institute of Technology, Cambridge, Massachusetts 02139, USA.
[2]Centro de Ciências Naturais e Humanas, Universidade Federal do ABC, Santo André, 09210-580 SP, Brazil.
[3]INFIQC, Departamento de Química Teórica y Computacional, Universidad Nacional de Córdoba, 5000, Argentina.
[4]Department of Materials Science and Engineering, Massachusetts Institute of Technology, Cambridge, Massachusetts 02139, USA.
[5]Department of Energy and Materials Engineering, Dongguk University-Seoul, Seoul, 04620, Republic of Korea.
[6]Department of Physics, Massachusetts Institute of Technology, Cambridge, Massachusetts 02139, USA.
[7]Department of Physics and Astronomy, The University of Alabama, Tuscaloosa, Alabama 35487, USA.
[8]Center for Materials for Information Technology (MINT Center), The University of Alabama, Tuscaloosa, USA.
[9] Natural Sciences Institute, Graduate Program in Physics – Federal University of Para, Belem, PA, Brazil.

ABSTRACT

The growth of large area single-layer graphene (1-LG) is studied using ambient pressure CVD on single crystal Ni(111), Ni(110) and Ni(100). By varying both the furnace temperature in the range of 800 - 1100 $^{\circ}$C and the gas flow through the growth chamber, uniform, high-quality 1-LG is obtained for Ni(111) and Ni(110) single crystals and for Ni(100) thin films. Surprisingly, only multilayer graphene (M-LG) growth could be obtained for single crystal Ni(100). The experimental results are analyzed to determine the optimum combination of temperature and gas flow. Characterization with optical microscopy, Raman spectroscopy and optical transmission support our findings. DFT calculations are performed to determine the energy barriers for diffusion, segregation and adsorption, and model the kinetic pathways for formation of different carbon structures on the low-index surfaces of Ni.

INTRODUCTION

The growth of carbon structures on different metallic/semi-metallic substrates has been extensively studied in the past decades [1-50]. Much of this research has focused on the formation of graphene on low-index nickel single-crystal surfaces, Ni(111), Ni(110) and Ni(100) [1-27, 43-46]. However, a complete microscopic understanding of the thermodynamic pathways for graphene formation on these surfaces is still lacking [15, 16, 30, 31, 46, 47, 51-57]. The growth of 1-LG on Ni(111) and Ni(110) surfaces has been reported, but similar explanations for the growth mechanisms on both surfaces is given. These explanations do not account for the distinctly different thermodynamic properties of the fcc (111) and (110) surfaces [1-27, 30, 31, 43-47, 51-57]. Advances in 1-LG growth techniques have been boosted by the isolation of 1-LG from

1

47 bulk graphite substrates [28], and recent research has shown the possibility of growing 1-LG and
48 multi-layer graphene (M-LG) on metals using CVD techniques without the added difficulty of ultra-
49 high vacuum environments and the subsequent transfer of such a material to dielectric substrates
50 [7-19, 29-32, 54-57]. The combination of process flexibility and high quality of the material
51 produced from these fabrication processes has enabled the integration of graphene into various
52 applications [33, 43-47, 51-57].
53
54 Although graphene has been grown successfully on a wide range of transition metals, copper and
55 nickel are the most widely used substrates [9, 43-47, 51-57]. Copper is the most frequently used
56 metal to grow monolayer graphene, since the low carbon solubility in Cu leads to a desirable self-
57 limiting surface growth of graphene [19, 32]. The same is not true for nickel (Ni), because the high
58 bulk solubility of carbon at typical high growth temperatures can result in a high rate of carbon
59 segregation and subsequent M-LG formation upon cooling. The growth of 1-LG on Cu, in general,
60 needs to be carried out under low pressure [34], further complicating the synthesis process and
61 adding to the cost of graphene production. The advantage to using nickel is that the growth of M-
62 LG can be avoided by selecting the proper growth conditions. Due to a stronger interaction
63 between graphene and Ni, only one graphene domain orientation exists for growth on Ni(111)
64 single crystals. So in this case, no tilt-grain boundaries are expected after a continuous and high-
65 quality film of graphene is formed [35].
66
67 The formation mechanisms of 1-LG are different for Cu and Ni. Growth of 1-LG in Cu is mainly
68 mediated by the adsorption of carbon atoms by the surface atoms followed by the diffusion of
69 such atoms across the surface and the formation of nucleation centers [34, 43-47, 51-57]. In Ni,
70 both bulk diffusion and surface diffusion leading to the formation of nucleation centers on the
71 surface most both be considered [1-5, 30, 34, 40, 41, 43-47, 51-57]. The growth of 1-LG graphene
72 on Ni is a crucial step toward the controlled growth of high-quality multi-layer graphene for a
73 number of technological applications [43-47, 51-57]. This motivates our study in order to further
74 optimize the growth conditions by building on the work of Seah et al., who demonstrated the
75 growth of bilayer graphene (2-LG) on Ni(111) by rapidly quenching the substrate after deposition
76 to limit the amount of carbon segregation [56].
77
78 In this work, we show that successful growth of 1-LG via ambient pressure CVD is achieved for
79 Ni(111) and Ni(110) single crystals and for Ni(100) thin films but only multilayer graphene (M-LG)
80 growth could be obtained for single crystal Ni(100). We characterize the different growth
81 mechanisms found on each orientation with optical microscopy, Raman spectroscopy and optical
82 transmission. DFT calculations are performed to provide an atomistic model of the processes
83 involved to support the experimental results. It is found that the formation of a uniform monolayer
84 on Ni single crystal substrates is epitaxially driven for the Ni(111) surface, while surface
85 thermodynamic and kinetic effects drive the formation on Ni(110) and Ni(100) by diffusion and
86 segregation of carbon atoms on Ni surfaces [2, 3, 5, 20]. The results and explanations provided
87 by this work are a step toward development of a means to control the number of graphene layers
88 formed on the surface.
89
90

METHODS

Experimental details

The Ni(111), Ni(110) and Ni(100) single crystal substrates used in this work (10mm in diameter, 1mm thick, 99.9995% purity) were obtained from Marketech International The substrates were electropolished further with a solution of glacial acetic acid and perchloric acid (60%) in the ratio of 7:3 by volume, to produce smooth substrate surfaces. X-ray diffraction measurements for each Ni substrate were performed after polishing to confirm the crystallographic orientation. The Ni(100) thin films used for the comparison study are approximately $1\mu m$ thick. The growth of graphene was performed using an ambient pressure CVD process. A 1-inch tube furnace is initially preheated to the growth temperature before the introduction of the Ni substrates contained within an open-ended silica tube. The substrates are then pre-cleaned by rapid heating under a flow of hydrogen at 1000 sccm. The temperature is then reduced to the growth temperature and methane gas at 100 sccm is added to the hydrogen flow. Exposure to methane continues for 300 seconds before removing the silica tube containing the substrates into a room temperature environment for a fast cool down. The graphene is then transferred from the substrates using a Poly(methyl methacrylate) polymer (PMMA) layer spin-coated on the surface followed by electrochemical delamination of the graphene/PMMA [48 -50]. The electrolyte consists of a 1M NaOH solution with a negative -10V applied on the Ni. The graphene layer can then be placed on a dielectric substrate and the PMMA can be removed by immersing in acetone [17].

Computational details

Density Functional calculations [58] were performed with the Quantum-Espresso Package [59] and the Perdew-Burke-Ernzerhof [60] Generalized Gradient Approximation as exchange-correlation functional. The ultrasoft pseudopotentials of the pslibrary [61] were used with plane-wave/charge density energy cutoffs of 40/320 Ry. To evaluate the interaction of carbon with each Ni surface considered, the unit cells were 3x3 squares for 100, $3x2\sqrt{2}$ rectangles for 110, and 3x3 hexagons for 111. The sampling of the first Brillouin zone was performed using grids centered at the Γ point, with a k-point density of 2x2x1. For the graphene monolayer coverage, the unit cells of the 100/110 surfaces were increased to 4x6 and $4x5\sqrt{2}$, creating an average strain in the graphene layer of less than 2%. Five Ni layers were used with additional 12 Å of vacuum in the perpendicular direction to avoid spurious interaction between periodic images. The energy and force thresholds adopted for the geometry optimizations were 0.0001/0.001a.u., respectively, and the bottom 2 Ni layers were kept frozen during ionic optimizations. Van der Waals corrections within the Grimme-2D method [62] were also considered.

RESULTS AND DISCUSSION

Figure 1 shows optical microscopy, AFM and Raman spectroscopy characterization of the 1-LG films obtained for Ni(111) and Ni(110) after transferring the 1-LG films to Si/SiO$_2$ substrates (note that 1-LG in Ni(100) thin films will be discussed later in the text). The optical images (Figures 1a and 1b) show a uniform contrast similar to samples derived from Cu foils [17-19, 23]. The observed optical color contrast corresponds to that estimated for 1-LG under the same theoretical model as was described previously [23]. The cross-sectional thickness of the film estimated from

135 the AFM tapping mode images in within the expected values of 1-LG, ranging from 0.48 to 0.57
136 nm (Figures 1c and 1d). Raman spectroscopy (Figures 1e and 1f) confirms the presence of
137 graphitic carbon in its monolayer configuration. Three main features are observed with 532 nm
138 laser wavelength excitation; the D, G, and 2D Raman peaks around 1350 cm^{-1}, 1580 cm^{-1} and
139 2700 cm^{-1}. The intensity ratio between the 2D and G peak intensities (I_{2D}/I_G) close to 2 and the
140 full width at the half maximum (FWHM) of the 2D band of ~ 30 cm^{-1} are spectroscopic signatures
141 of the presence of 1-LG. Differences in the D-band intensity (marked with an asterisk), suggest
142 that 1-LG grown on Ni(110) is structurally more disorganized then the corresponding film on
143 Ni(111). Further confirmation of the presence of 1-LG and of its quality when grown on Ni(111)
144 and Ni(110) catalysts was done by measuring the optical transmittance of the films over the visible
145 range (Figure 2d). The films were transferred to quartz substrates and the average transmittance
146 was measured to be approximately 97.8% for 1-LG grown on both Ni(111) and Ni(110). This value
147 is within experimental error of the expected transmission for 1-LG of 97.7% [23]. The
148 transmittance was also found to be nearly the same to that measured for 1-LG grown over a Cu
149 foil following the growth process described elsewhere [36, 37].
150
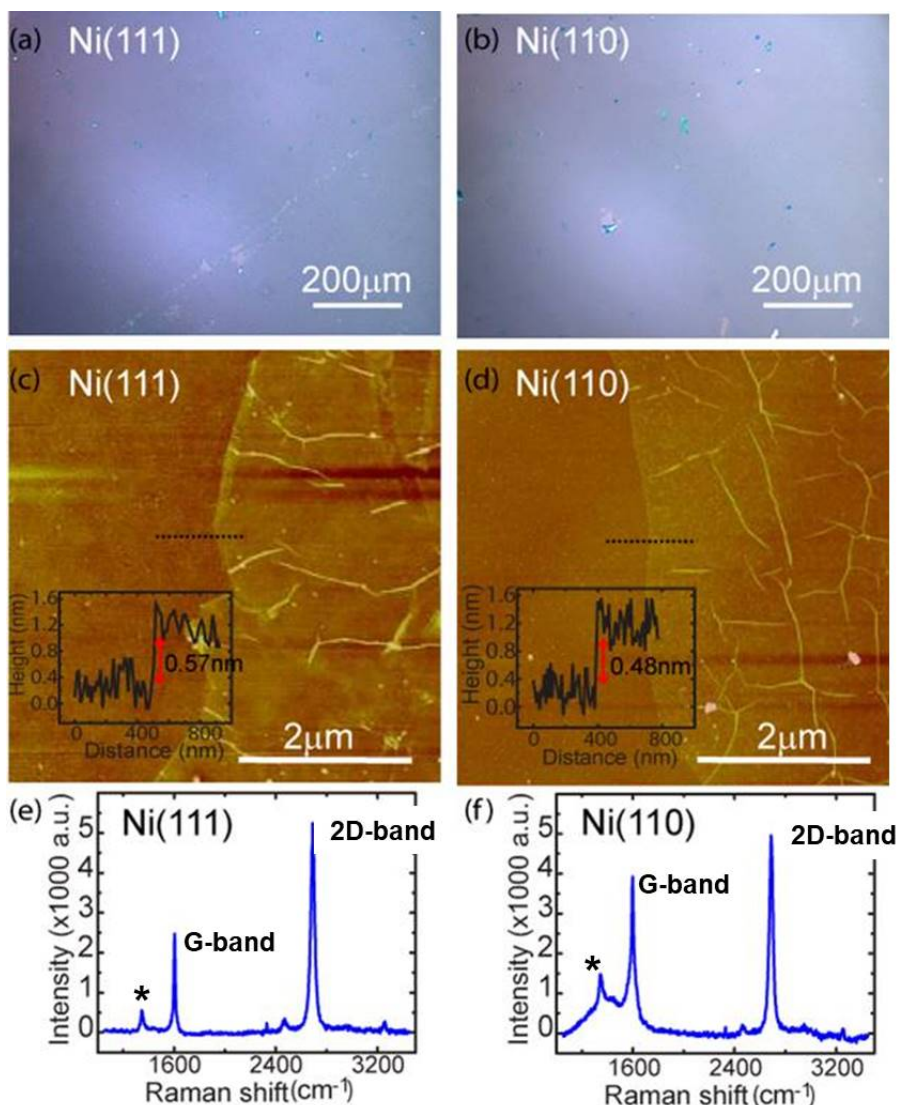
Figure 1. Optical microscopy images of 1-LG grown on (a) Ni(111) and on (b) Ni(110) after transferring the 1-LG layer to a Si/SiO$_2$ substrate. AFM images of the edge of typical 1-LG graphene films transferred to Si-SiO$_2$ for 1-LG grown on (c) Ni(111) and (d) Ni(110). The insets reveal the formation of 1-LG in each case.and Raman spectra are shown for 1-LG grown on (e) Ni(111) and (f) Ni(110).

The process parameters are of significant importance for the success of 1-LG growth on Ni(111) and Ni(110) single crystals. As illustrated in Figure 2f, polishing the surface of Ni pieces (as described in the Methods section) was critical for 1-LG preparation due to the observed formation of M-LG under the same processing conditions on samples rougher than a few nanometers. Formation of M-LG can be attributed to the preference of graphene formation on Ni step edges, which are more abundant on rougher crystalline surfaces [25, 38, 39]. Growth on a rough surface results in the overlap of islands originating from neighboring step edges [1-5, 35, 38]. Figures 2(a) through (c) show Atomic Force Microscopy (AFM) images of clean and polished surfaces for Ni(111), Ni(100) and Ni(110) before graphene growth. The surface roughness is the largest for Ni(110) and the smallest for Ni(111). None of the surfaces prepared using our method were rough enough to prevent monolayer growth. The inset in Figure 2f shows the X-Ray Diffraction (XRD)

measurements taken from the Ni(111), Ni(110) and Ni(100) single crystals, confirming their crystallographic directions.
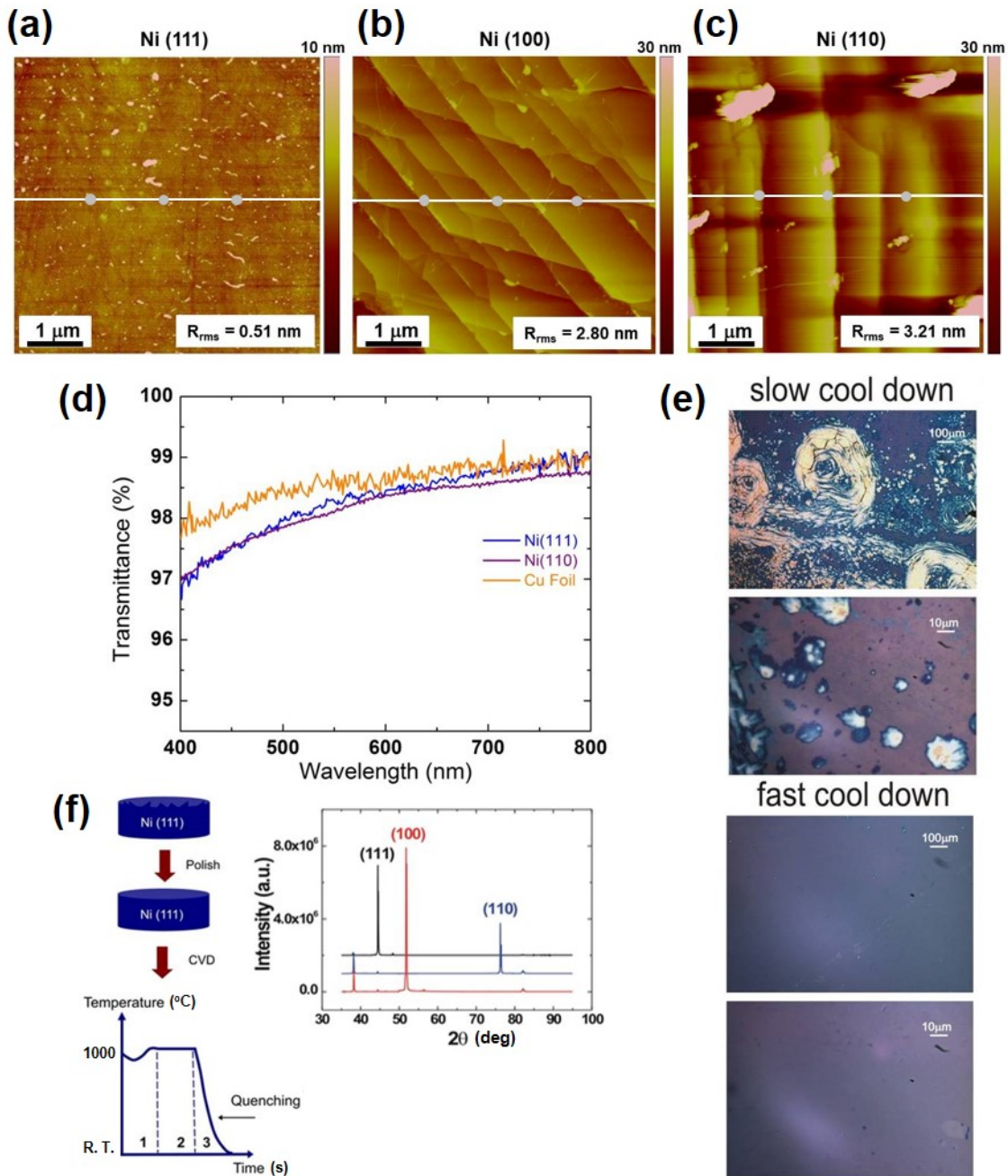
Figure 2. Atomic Force Microscopy (AFM) images of clean and polished surfaces for (a) Ni(111), (b) Ni(100), and (c) Ni(110) before graphene growth. The solid lines and spaces between bullets indicated, respectively, where a surface profile line was taken and regions where roughness analyses were performed. The roughness (R_{rms}) reported in the bottom right corner is an average of values taken in several different regions. (d) Optical transmittance across the wavelength range of 400-800 nm for 1-LG films grown from Ni(111) (blue), Ni(110) (purple) and Cu foil (orange). (e) Images of samples obtained for Ni(111) using fast and slow cool down from T=1000 °C. Fast quenching produces a more continuous film of 1-LG, while slow quenching produces an inhomogeneous film composed of few layer flakes and fragments. (f)

6

179 Schematic of the processing steps for growing 1-LG from Ni single crystal. R.T. stands for room
180 temperature. The inset shows the XRD measurements of the Ni(111), Ni(110) and Ni(100) single crystals.
181
182 The cooling rate for temperature quenching of the Ni plays a significant role in the crystalline
183 structure of the resulting sample. A fast cool down prevents the formation of a graphite phase
184 after the monolayer forms on the Ni surface (bottom panel in Figure 2e). Slow cooling results in
185 films consisting mostly of M-LG (top panel in Figure 2e). In addition, the selected growth
186 temperature (T) must be correct to achieve 1-LG formation on Ni. For the same gases and flow
187 rates (H_2=1000 sccm, CH_4=100 sccm) and growth time (t=5 min), the optimum growth
188 temperature T depends on surface orientation. We found that 1-LG on Ni(111) is formed at
189 T=(1000±1) $^{\circ}$C. In contrast, M-LG is formed on the Ni(110) and Ni(100) surfaces, as shown in
190 Figures 3d, 3e and 3f. For a growth temperature of T=(800±1) $^{\circ}$C, 1-LG is formed on Ni(110) and
191 M-LG is formed on Ni(111) and Ni(100), as shown in Figures 3g, 3h and 3i. For the experimental
192 conditions investigated in this work, 1-LG was not formed on a Ni(100) single crystal, but 1-LG
193 was formed on Ni(100) thin films. For the deposition temperatures investigated below 800°C, no
194 ordered carbon structures were formed on any of the Ni surfaces, independent of their
195 crystallographic orientation. Table 1 summarizes the results for Ni single crystals.
196
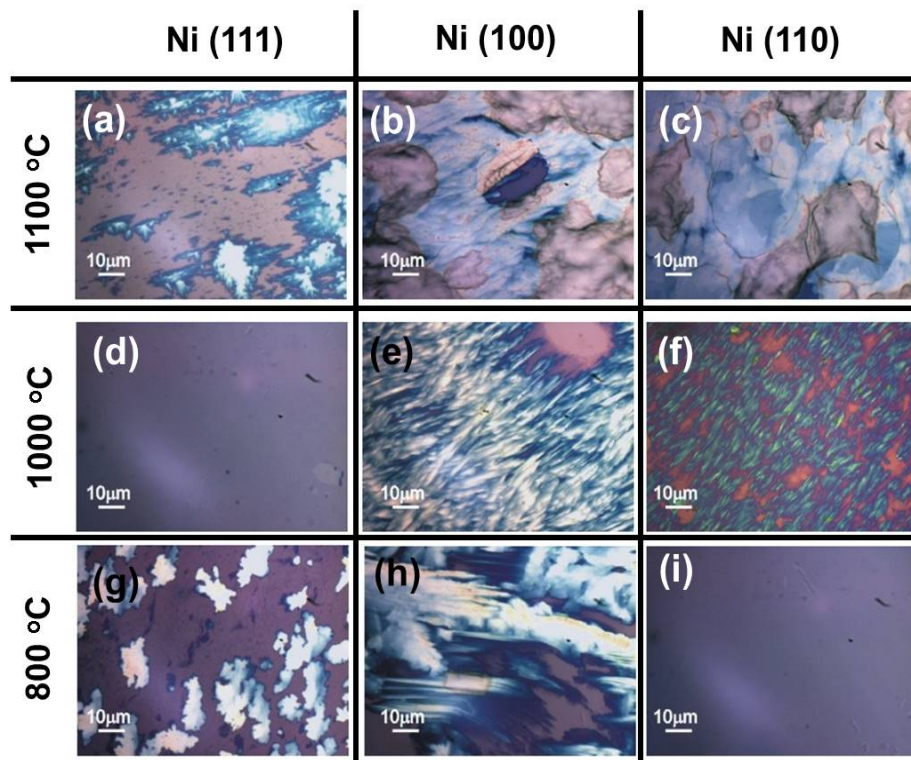
197
198 **Figure 3.** Optical absorption images of graphene grown on the Ni(111), Ni(100) and Ni(110) at
199 temperatures of 800, 1000 and 1100 $^{\circ}$C. Multi-layer graphene is obtained in all cases, except for (i) Ni(110)
200 at 800 $^{\circ}$C and (d) Ni(111) at 1000 $^{\circ}$C, where 1-LG is obtained.
201
202

Table 1. Summary of the growth of carbon structures at different temperatures and different crystallographic directions using gas flow rates of 1000 sccm for H_2 and 100 sccm for CH_4. 1-LG is single-layer graphene and M-LG is multi-layer graphene.

	Ni(111)	Ni(110)	Ni(100)
1100 °C	M-LG in single crystal	M-LG in single crystal	M-LG in single crystal
1000 °C	1-LG in single crystal	M-LG in single crystal	M-LG in single crystal and 1-LG in thin film
800 °C	M-LG in single crystal	1-LG in single crystal	M-LG in single crystal
750 °C - 790 °C	None	None	None

Growth of 1-LG on Ni(111)

Nickel crystals are Face Centered Cubic (FCC) structures with a bulk lattice parameter of 3.52 Å. Ni(111) has a surface lattice parameter of $a_{Ni(111)}$ = 2.49 Å while 1-LG is a nearly perfect match with a_{1-LG} = 2.46 Å [1-5]. Compared to the other two orientations, Ni(110) and Ni(100), Ni(111) has the highest atomic packing density [41, 63] and the smallest surface energy, $S_{Ni(111)}$ = 1606 ergs.cm^{-2} versus $S_{Ni(110)}$ = 2057 ergs.cm^{-2} and $S_{Ni(100)}$ = 1943 ergs.cm^{-2} [1-5, 64]. Since the surface energy is related to the strength of the C-Ni interaction, we expect that the carbon adsorption energy and energy barriers E_{across} for the diffusion across the surface [40-42, 65] to be related to $S_{Ni(111)}$, which means that they should be lower in this (111) face. Diffusion of carbon atoms will also be dependent on its surface mean-free path. If the density of C atoms increases, the mean free path decreases, making diffusion less likely since dimers have reduced mobility. The C deposition rate is proportional to the reactivity rate of methane and is the smallest on Ni(111) at all temperatures [1-5].

For Ni(111) 1-LG was obtained at T=(1000±1) °C, while M-LG was obtained at T=(1100±1) °C and at T=(800±1) °C and no carbon structure formation was observed for temperatures below (790±1) °C (we have studied temperatures between 750 °C and 800 °C in steps of 10 °C). At the optimum growth temperature of (1000±1) °C, the driving phenomena behind the growth are balanced, mainly the deposition rate, diffusion across the surface, diffusion into the bulk and segregation during cool down. An additional factor is that CH_4 reactivity is above a minimum threshold at this temperature, but this is already the case at 800 °C (see Table 1).

At 800 °C, bulk diffusion is significantly lower compared to 1000 °C and, consequently, the segregation during the fast cool down is inhibited. Diffusion of carbon atoms into the bulk at 1000 °C and the limited segregation during rapid cooling control the density of carbon atoms for the Ni(111) surface, thereby allowing 1-LG formation. At higher temperatures such as 1100 °C, the probability of carbon atom diffusion across the surface and the probability of carbon atom diffusion

236 into the bulk are approximately equal and the flux of carbon atoms diffusing into the bulk is larger.
237 In addition, cooling from 1100 °C takes longer, resulting in increased carbon segregation during
238 the cooling down process, so M-LG was preferentially obtained on Ni(111).
239
240 By changing process parameters for temperatures between 780 °C and 1000 °C, the growth of
241 monolayers on Ni(111) is possible. Below 1000 °C, the deposition rate and the sticking coefficient
242 of carbon on the Ni substrate decrease, so obtaining M-LG between 1000 °C and 780 °C probably
243 means that the flow of CH_4 is still too high in such cases, even though the deposition rate
244 decreases (diffusion into the bulk is increasingly suppressed as the temperature decreases). So
245 by substantially decreasing the CH_4 flow, 1-LG is expected. In Figure 4(a)-(c), it is demonstrated
246 that mostly 1-LG can be obtained at 900 °C if the CH_4 flow is reduced from 100 to 50 sccm, while
247 the H_2 flow is kept at 1000 sccm and a rapid cool down is used. Figure 4(d) shows the Raman
248 spectrum for the 1-LG grown under such conditions.
249
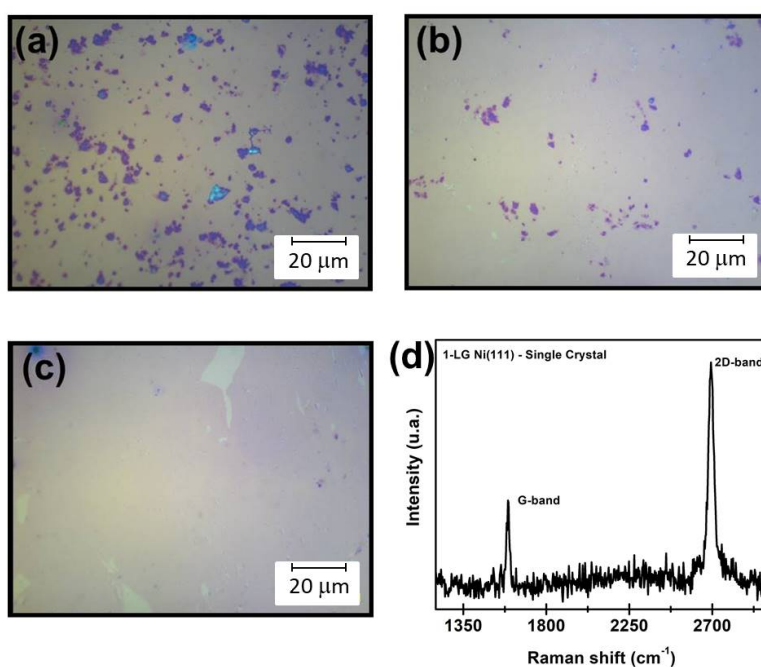
250
251 **Figure 4.** Optical images of the graphene films obtained from Ni(111) at T=900 °C and gas flows of H_2 =
252 1000 sccm and (a) CH_4 = 100 sccm, (b) CH_4 = 75 sccm and (c) CH_4 50 sccm. 1-LG is formed when the
253 flow of methane is decreased from 100 sccm to 50 sccm. (d) Raman spectrum for the 1-LG shown in (c).
254
255 Our computer simulations suggest that 1LG on Ni(111) has a planar structure, with half of the
256 carbon atoms attached to an on-top position and the other half attached to a hollow-hcp position,
257 as shown in Figure 5. Although we present this structure as the most stable, there is still
258 disagreement about the best atomic arrangement of graphene on Ni(111). In fact, it has been
259 shown that more than one structures may coexist [9, 66, 67], due to the very low energy difference
260 between them. The structural and energetic parameters are listed in Table 2.
261

top view   **side view**

Ni(111)

Ni(110)

Ni(100)
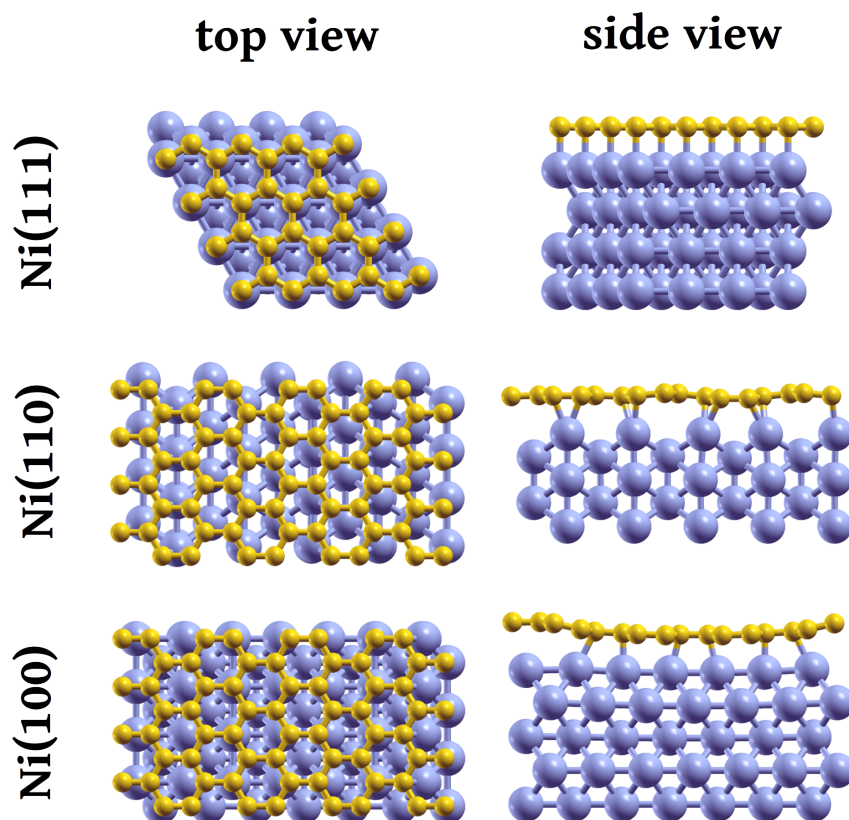
Figure 5. 1-LG on nickel, in its optimized configuration. In yellow, carbon atoms and in blue, nickel.

Table 2. Energetic and structural information of 1-LG on different crystal planes as obtained by DFT calculations, shown in Fig. 05. The values show the average adsorption energy by atom, the average carbon-surface distance and the maximum buckling on the graphene layer.

	E_{ads} (meV.at^{-1})	$d_{graph\text{-}surf}$ (Å)	buckling (Å)
Ni(111)	164	2.11	0.00
Ni(110)	209	2.03	0.29
Ni(100)	180	2.13	0.69

Suggested model for carbon growth on Ni(111)

We have calculated the adsorption energy of a single carbon atom on a perfect Ni(111) surface, emulating the low concentration regime, corresponding to the initial stages of growth (see Figure 6). Nearly all generated carbon will diffuse laterally until a dimer is formed. Trimers and tetramers are less stable than dimers, so probably the first stages of the growth will involve only dimers. The best site for carbon adsorption on the surface is on a hollow site, in agreement with theoretical results from the literature [68, 69] (for more information about the structures and the way of calculating the adsorption energies, please see the Supplemental Material [70]). The carbide

279 position, corresponding to carbon absorption is more stable by 0.42 eV. For a second C atom,
280 there is a 0.33 eV gain in forming a dimer, instead of adsorbing far away from the first C atom. All
281 the adsorption energies for a single carbon atom, as well as the structural parameters for the
282 configurations, are presented in Table S1. To obtain an entire picture of the processes involved
283 in the first stages of carbon deposition, we have also evaluated the diffusion barrier for diffusion
284 across (E_{across}) and into the surface (E_{into}), as well as dimer diffusion across the surface. Figure
285 7a illustrates the main paths considered and Figure 7b quantifies them, showing that E_{across} barrier
286 is less than half of E_{into}.
287
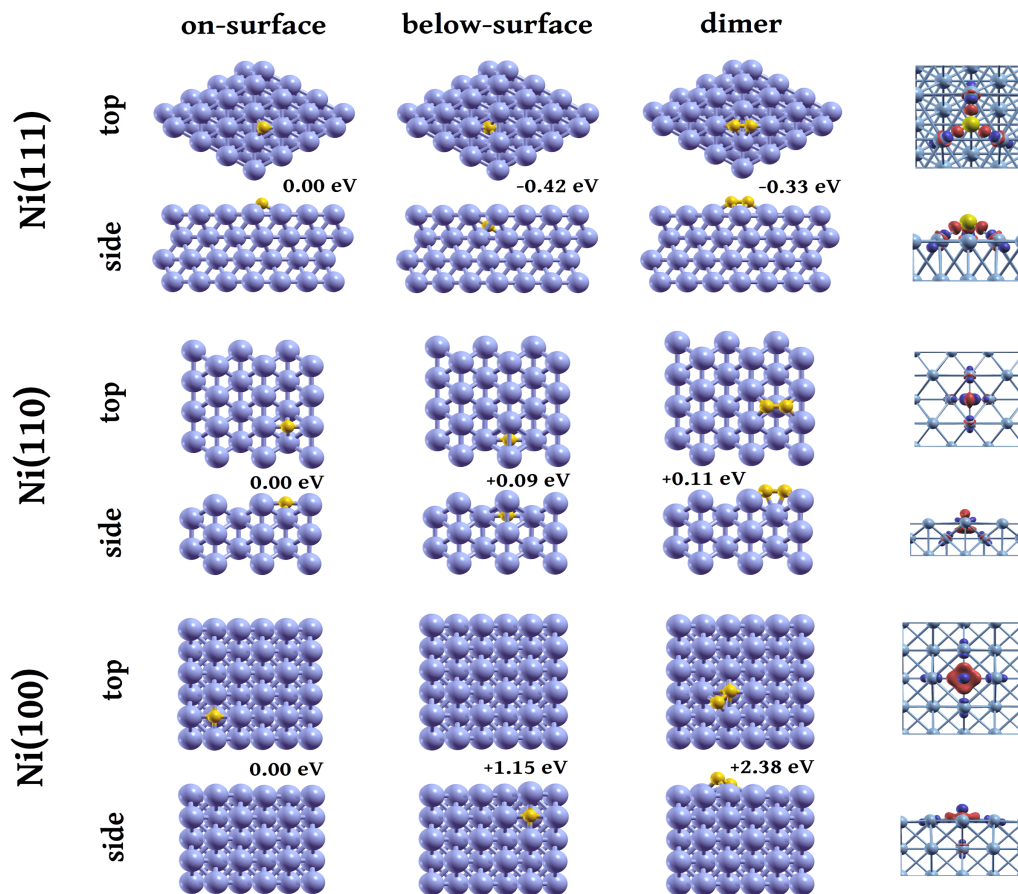
288
289 **Figure 6.** The most stable sites for (from left to right): carbon adsorption, carbide formation, and dimer
290 formation on different Ni crystal planes. The color code is the same as in Figure 5. The relative adsorption
291 energies for each surface are displayed, and in the case of dimers, the value corresponds to the energy
292 variation with respect to the adsorption of two isolated C atoms. On the right, the charge density difference
293 for single atom adsorption is shown. In these plots, red/blue means electron accumulation/depletion.
294

295 With these experimental and theoretical results in mind, we propose a possible scenario for
296 graphene formation on Ni(111). At the low coverage regime, the incoming C atoms should adsorb
297 at the surface and diffuse across the Ni surface at a much higher rate than into the Ni bulk. If the
298 deposition rate is large enough and the temperature is low enough to inhibit diffusion into the bulk,
299 then the adsorbed C atoms should preferentially form dimers. Dimers are more stable than
300 monomers, and it is nearly impossible for a dimer to diffuse into the bulk. Dimers may form trimers

301 with incoming C atoms and the dimers can also diffuse across the surface with a somewhat higher
302 activation energy of around 0.6 eV. Formation of a monolayer will depend mostly on a delicate
303 balance of the deposition rate and the temperature. We also note that the formation of a carbon
304 cluster on Ni(111) is favored by symmetry (see Figure 6), since Ni(111) has a surface with
305 hexagonal regularity and a lattice parameter very close to that of 1-LG.
306
307 Following the work by Ozcelik [31], it is possible that the atoms attached to the edges of the
308 clusters will form pentagons and heptagons that will grow and heal themselves forming hexagons
309 by a Stones-Wales-Thrower mechanism. The connection among the several nucleation centers
310 is likely to occur through this process. From these considerations, Ni(111) is expected to provide
311 the best quality graphene. At low growth temperature (800 ℃), surface diffusion of carbon atoms
312 dominates, so eventually M-LG will grow. For higher temperatures (1000 ℃), bulk diffusion
313 dominates and less surface carbon concentration is expected. Dimer diffusion will become more
314 probable, and dimers would connect and generate 1-LG. Finally, if the temperature is too high
315 (1100 ℃) the fast reactivity of CH_4 will generate a higher carbon concentration at the surface, so
316 M-LG will grow. Although our calculations suggest that the growth of nucleation centers goes by
317 the formation of dimers, the formation of nucleation centers by dimers was unclear until recently:
318 Patera *et al.* [71] demonstrated via experiments and DFT calculations that the 1-LG growth
319 process occurs by the addition of carbon lines parallel to the graphene edge always involving a
320 kink site and a Ni adatom. The participation of Ni adatoms is energetically favored since it reduces
321 the rate limiting energy barriers by approximately 35% (according to their calculations it lowers
322 from 2.46 to 1.61 eV). Therefore, Ni adatoms spontaneously bind to kink sites in the graphene
323 edge, and act as single atom catalysts where carbon atoms stabilize the attachment of Ni
324 adatoms. This consequently promotes the addition of carbon atoms in the edge formation. Based
325 on our calculations we propose that, even though the range of temperatures in our experiments
326 is different, the formation of graphene domains follow the same trends.
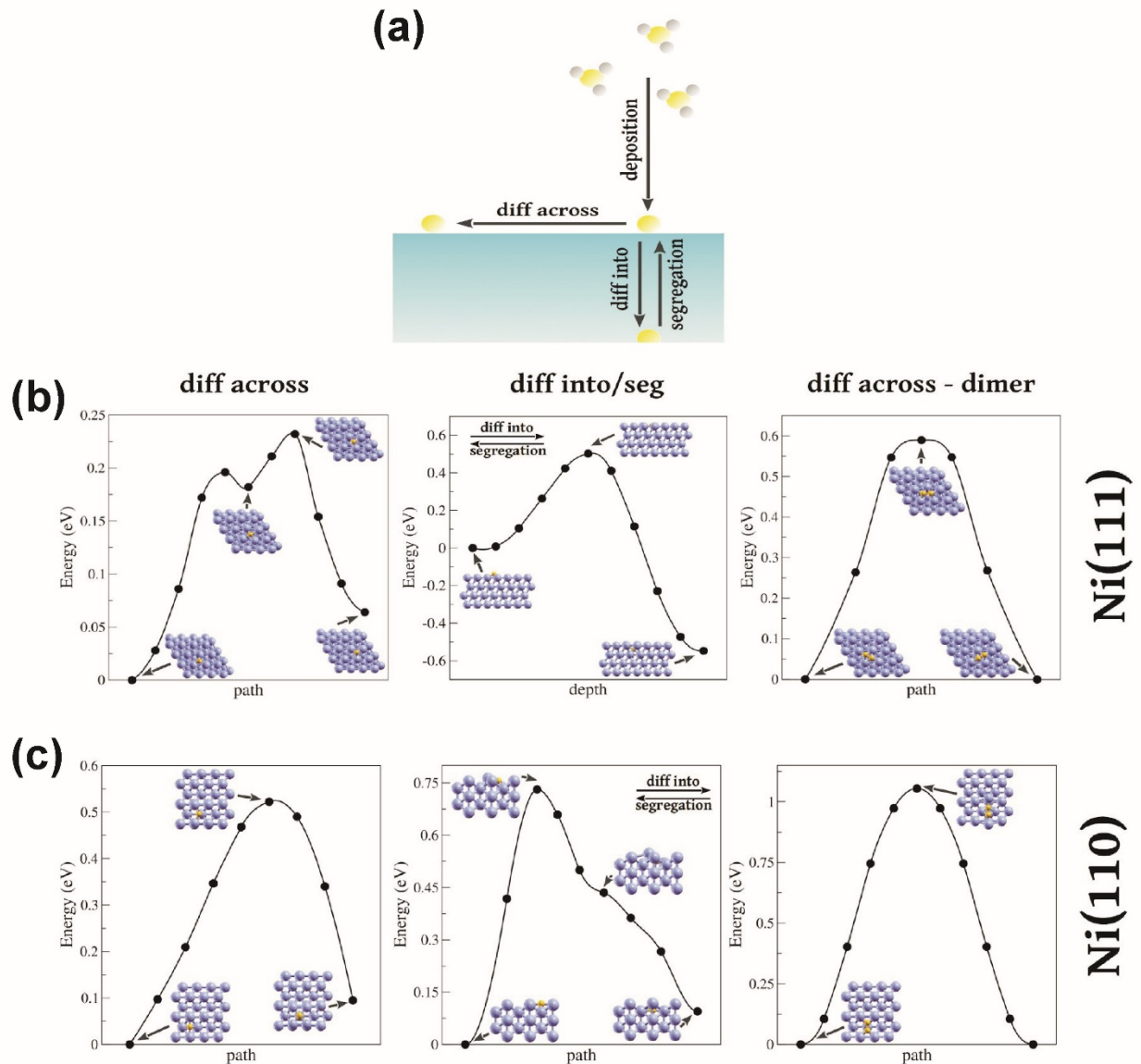
Figure 7. Diffusion of carbon on a nickel surface. In (a) all the processes involved at the first stages of graphene growth on nickel are depicted. In (b) and (c) the kinetic barriers for diffusion across and into (or segregation, in reverse) for a single carbon atom and diffusion across for a dimer, on the 111 and 110 planes, are shown. The color code is the same as in Figure 5. For the case of Ni(100) all the barriers are higher than 1 eV, so they are not shown.

Growth of 1-LG on Ni(110)

C-C bonds are expected to lead to the formation of monolayer graphene on the 110 surface, however a complete understanding of the routes leading to the formation of a stable and large area of a graphene monolayer has been elusive [1-5,13-15,38, 43]. The Ni(110) surface has the lowest atomic packing density. The C deposition rate ($R_{Ni(110)}$) and the surface energy for Ni(110) are the largest compared to the 111 and 100 directions. On Ni(110) with gas flows of 1000 sccm for H_2 and 100 sccm for CH_4 with rapid quenching after deposition, 1-LG was obtained at (800±1) ^oC, M-LG was obtained at (1000±1) ^oC and (1100±1) ^oC and no carbon structure formation was observed below 790 ^oC (see Table 1).

344

345 Films of 1-LG will be incommensurate with the Ni(110) surface and this results in Moiré patterns
346 [13, 14]. In addition, the carbon nucleation sites have different orientations, producing multiple
347 graphene domains. As a consequence, graphene in Ni(111) is expected to have poorer quality
348 relative to that grown on the 111 plane. The Raman spectrum in Figure 1f shows a significant D-
349 band intensity for 1-LG grown on Ni(110), while Figure 1e shows a very weak D-band intensity
350 for 1-LG grown on Ni(111). Our computer simulations suggest that the graphene monolayer
351 formed on a perfect Ni(110) surface is not planar, but has a buckling due to the different C-Ni
352 bonds formed due to the mismatch between the two structures. The best configuration found is
353 shown in Figure 5, and the energetics and structural data are shown in Table 2. A complete model
354 that describes the dynamics of 1-LG formation in Ni(110) is yet to be developed, but recent
355 information regarding diffusion and segregation may further this effort [1,15].

356

357 **Suggested Model for carbon growth on Ni(110)**
358 Our computer simulations results suggest that carbon atoms would preferably attach to a bridge-
359 001 site (see Figures 6 and S1 for details). The carbide formation is slightly disfavoured, but only
360 by 0.09 eV. On this plane, the energy barriers to diffuse across the surface or into the bulk are
361 closer (0.53 eV for across and 0.72 eV for into), and we expect these two processes to compete
362 more compared to the 111 case. Paths and kinetic barriers are shown in Figure 7c. The arrival of
363 a second C atom creates a competition between dimer formation and isolated adsorption since
364 they have very similar energies, as shown in Figure 6. Trimers and tetramers are less stable than
365 dimers and are not likely to be formed. Therefore, at the low coverage regime, the 110 face shows
366 more balanced thermodynamics, with dimer formation, diffusion and segregation in close
367 competition with each other.

368

369 The incommensurability of graphene with the substrate may reinforce growth through the healing
370 mechanism of pentagons and heptagons [31]. On the other hand, the lack of hexagonal symmetry
371 of this face may result in graphene domains growing from different nucleation sites joining with
372 different orientations. As a consequence, we would expect graphene with poorer quality relative
373 to the 1-LG grown on the 111 direction. Electrical measurements should also confirm these
374 statements about the quality of the 1-LG grown on the different Ni surfaces. However, to the best
375 of the authors' knowledge, there are no such measurements in the literature focusing on the
376 quality of graphene formed in each direction.

377

378 In summary, we suggest that a carbon on the 110 plane can diffuse across the surface or into the
379 bulk with nearly the same likelihood because the barriers for both processes are similar. At 800ºC
380 this balance allows the surface to have a moderate carbon concentration with enough time to
381 order. Also the bulk should not saturate, and segregation is not likely to occur. Dimers are slightly
382 less stable than monomers, so atomic carbon is available to diffuse into the bulk while carbon
383 concentration is low. After reaching a threshold coverage, carbon atoms dimers will be more
384 prevalent and graphene would grow. The symmetry of the plane does not favor the formation of
385 highly ordered graphene. When temperature is increased (1000ºC) the reaction rate of CH_4
386 increases and the resulting high carbon concentration produces M-LG.

387

Growth of M-LG on Ni(100)

Epitaxial growth of 1-LG is more complicated than the previous cases due to the larger mismatch between graphene and Ni(100) surface. The C deposition rate ($R_{Ni(100)}$) and the surface energy for Ni(100) are smaller compared to the 110 direction but are larger compared to the 111 direction. Our computer simulations predict that, if formed, a graphene layer on the Ni(100) surface would not remain planar, but would have a large corrugation due to the mismatch between the two structures (graphene has a honeycomb structure while the Ni(100) surface has a square symmetry). These undulations prevent some of the carbon atoms to be directly linked to the metallic surface, as shown in Figure 5. Theoretical simulations from the literature [72] have also obtained these undulations, that may vary in amplitude between 0.2 Å to 1.0 Å depending on the graphene position and orientation with respect to the Ni surface, and also the size of the unit cell used in the simulation. In our experiments, even though we tested different growth parameters, such as temperature and gas flow, 1-LG was not obtained on Ni(100). To grasp why graphene is not formed, we need to understand better how carbon interacts with the Ni atoms at the surface when adsorbed or segregated.

We performed DFT calculations of the adsorption energy of individual carbon atoms on the 100 plane, finding that the most stable site is the hollow one (see Figures 6 and S1 for details). Observing the charge density difference plots (displayed in Figure 6) and Bader charges for the three surface planes (-0.70 for C on Ni(111), -0.83 for C on Ni(110) and -0.99 for C on Ni(100)), we can deduce that the C-Ni bonds on the 100 face are stronger and more localized than on the 111 and 110 planes. This charge localization would inhibit dimer formation, due to the fact that this new C-C bond would weaken the strong C-Ni and Ni-Ni already existing bonds. This disruption in the nickel orbitals (related to spin unpairing) would take the Ni crystal out of its energy minimum [1-5, 28, 38, 40, 41]. Our calculations show that the dimer formation is highly unlikely at low coverages (dimer formation is 2.38 eV higher in energy than two carbon atoms separately adsorbed), and this is also prevented by symmetry.

The large adsorption energy difference between sites (all listed in Table S1) makes lateral diffusion unlikely, with barriers in the order of 2.17 eV. Although the 100 surface is more open than the 111 plane, diffusion into the bulk is less likely in the low coverage regime (below 0.5 monolayer coverage, where C-C bonds should be disfavored) because the carbide phase with the carbon atom below the surface is very unstable (1.15 eV higher in energy than a carbon on a surface hollow site). At appoximately 1 monolayer coverage or larger, carbon may enter the surface and create lattice disorder. Dimers are not likely to form as evidenced by prior work investigating segregation of carbon on Ni(100) surfaces that show monomers are well described by the Langmuir model where only non-interacting solute atoms are taken into account [1-5, 28, 38, 40, 41, 45]. According to Porter et al. [1], segregation of C atoms to the surface of Ni(100) is reversible at monolayer coverages, confirming that C atoms at the surface are weakly interacting with each other.

Most theoretical predictions [1-5, 9, 20, 30, 31] point out that Ni(100) is unlikely to allow any formation of an organized carbon structure. At high carbon saturation levels, occuring at sufficiently high temperatures (above 800 °C in this work), M-LG structures are obtained on this

432 face. Indeed, after CH_4 breaking at the 100 surface, the carbon atoms attach strongly on the
433 hollow sites (tetra-coordinated). These bonds are highly localized. Diffusion across and into are
434 not likely to occur in the low coverage regime, because the barriers are very high. Dimers would
435 not form, because the C-Ni bond is too strong when compared with a possible C-C bond. As the
436 carbon concentration increases all the processes would start to compete. Some of the atoms
437 would diffuse into the surface, and others would attach to the pre-existing Ni-C layer. When
438 saturation is reached, segregated C atom would attach to the surface carbon layer from below.
439 The plane symmetry and the high carbon concentration (even at low temperatures) will favor the
440 precipitation of M-LG.
441
Growth of 1-LG on Ni(100) Thin Films
442
443 Rasuli et. al [15] performed theoretical calculations simulating CVD growth of graphene on
444 Ni(100). They predict that by varying the flux of gases and temperatures it is possible to grow
445 high-quality monolayer graphene. In the present work, we varied the temperature up to (1100±1)
446 ^{o}C and varied the gas flux but we did not observe any carbon monolayer structure formation for
447 Ni(100) single crystals. A possible explanation for predicted monolayer formation (and not
448 multilayer formation) could be related to the fact that only four layers of Ni were used to represent
449 the substrate, limiting a complete description of the diffusion into the substrate and segregation
450 that might occur at these temperatures. In their calculation, strong Ni-C interactions may be
451 underestimated at the low coverage regime, as opposed to our findings that show these are
452 essential for predicting the formation of carbon structures using a Ni(100) catalyst.
453
454 More recently, Zou *et al.* [72] demonstrated via experiments the successful growth of 1-LG for
455 Ni(100) single crystals and on Ni(100)-oriented domains of 1μm thick polycrystalline Ni(100). Their
456 DFT calculations assume the interaction of a pre-existent monolayer with the Ni surface and are
457 in good agreement with ours, as shortly described above. These experiments [72] motivated us
458 us to perform experiments on 1μm-thick Ni(100) thin films. We applied the same growth conditions
459 as for the Ni(100) single crystals, and for the same gases and flow rates (H_2=1000 sccm, CH_4=100
460 sccm) and growth time (t=5 min), we successfully obtained 1-LG on Ni(100) films using the rapid
461 cool down procedure from a growth temperature of 1000 ^{o}C. Note that our results complement
462 their findings since the growth temperature and the carbon source used here are different: their
463 growth temperatures range from 400 to 600 ^{o}C and they use ethylene (C_2H_4) as a carbon source
464 [72]. Figures 8(a) through (c) summarize our analysis of the 1-LG obtained from 1μm Ni(100)
465 films, in good agreement with the analysis of the 1-LG obtained from Ni(111) and Ni(110), as
466 discussed above.
467
468 Explaining the differences between thick and thin Ni films that lead to successful monolayer
469 growth in thin films is an ongoing work that will be reported elsewhere. The different behavior may
470 be because the top and bottom surfaces are no longer isolated from one another and may
471 mutually interact. Therefore, the energy renormalizations related to the C-Ni and Ni-Ni bonds
472 would no longer be local. This could change the activation energies for the diffusions into bulk
473 and across the surface, the surface energies and adsorption energies. Another possibility is that
474 the total amount of carbon dissolved in the Ni film is proportional to the thickness, so less carbon
475 would then segregate to the surface in thinner films.

476

1-LG Ni(100) – Single Crystal – Thin Film – SiO₂
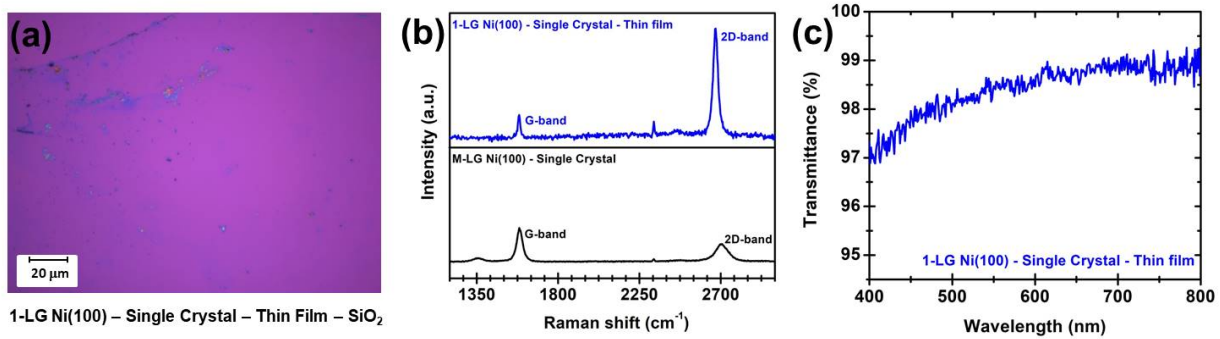
477

478 **Figure 8.** (a) Optical image of the 1-LG obtained for Ni(100) films with thickness around 1μm using fast cool
479 down approaches starting at T=1000 °C. (b) Top panel: Raman spectrum of the 1-LG imaged in (a). Bottom
480 panel: for comparison, the Raman spectrum of the M-LG obtained for the Ni(100) single crystal discussed
481 in the previous section. (c) Optical transmittance across the wavelength range of 400-800 nm for 1-LG films
482 grown from 1μm thick Ni(100) films.

483

484 **Non-occurrence of carbon structures at low temperatures (T<800 °C)**
485 For the three studied crystallographic directions, no carbon structures were grown below 790 °C
486 with gas flow rates of 1000 sccm for H_2 and 100 sccm for CH_4 and an exposure time of 300 sec
487 follwed by rapid quenching. The lack of carbon structure formation is mainly due to the decrease
488 in the methane reactivity rate as the temperature decreases. A decrease in temperature of about
489 200 °C results in the decrease of CH_4 reactivity by more than an order of magnitude [26]. One
490 way to overcome this decreased reactivity would be to increase the exposure time (or
491 equivalently, to increase the concentration of CH_4. The use of other hydrocarbons for graphene
492 growth at temperatures lower than 800 °C on Ni has been reported by several authors [13, 14,
493 46, 47]. Even though diffusion into the bulk, diffusion across the surface and segregation also
494 dramatically decrease below 790 °C, we do not believe that this limits the growth, since these
495 processes have been observed to occur at temperatures as low as 350 °C. [1, 16]

496

497 **CONCLUSIONS**

498

499 In this combined experimental-theoretical study, we have demonstrated that Ni(111) and Ni(110)
500 can be efficiently used to grow single-layer graphene (1-LG) under ambient pressure CVD, over
501 areas on the order of a few cm^2. Upon transferring the films to dielectric substrates, our
502 measurements confirm the presence of 1-LG on Ni(111) and Ni(110). Using the same gas flow
503 rates and growth times, different temperatures are needed to grow 1-LG on Ni(111) (T=(1000±1)
504 °C) and on Ni(110) (T=(800±1) °C). We have also performed DFT calculations to suggest
505 atomistic models to explain the growth of graphene on the different low-index surfaces. We
506 propose that crystal symmetry, adsorption energies, diffusion across, diffusion into, segregation,
507 and dimer formation are the key factors needed to formulate a description of the first stages of
508 graphene growth. For Ni(100) the formation of 1-LG is not favored by symmetry and is also
509 adversely affected by the very strong and localized Ni-C bonds that inhibit C-C dimer formation.
510 However, we show that M-LG can be formed on Ni(100), in disagreement with previous
511 predictions suggesting that organized carbon structures on Ni(100) were unlikely or not possible.
512 Therefore our discussion is very relevant to current research efforts in graphene fabrication and

applications, especially when low temperature growth is desirable. Although only M-LG was obtained on Ni(100) single crystals, with 1-LG obtained for 1μm thick thin films, complementing recent results by Zou *et al.* [72]. Due to the ease of multilayer growth on Ni, this study shows promise for extension to control the number of layers formed on different Ni surfaces, an added benefit for different technological applications.

AUTHOR INFORMATION

*Corresponding authors:
paulo.t.araujo@ua.edu, f.ribeiro@ufabc.edu.br, jimenaolmos@gmail.com

ACKNOWLEDGMENTS

REFERENCES

[1] Blakely, J. M.; Kim J. S.; Potter, H. C. (1970) Segregation of Carbon to the (100) Surface of Nickel. J. Appl. Phys. 41 (6): 2693-2697.

[2] Isett, L. C.; Blakely, J. M. (1975) Binding energies of carbon to Ni(100) from equilibrium segregation studies. Surface Science 47 (2): 645-649.

[3] Isett, L. C.; Blakely, J. M. (1976) Segregation isosteres for carbon at the (100) surface of nickel. Surface Science 58 (2): 397-414.

[4] Schouten, F. C.; Gijzeman, O. L. J.; Bootsma, G. A. (1979) Interaction of Methane with Ni(111) and Ni(100); Diffusion of Carbon into Nickel through the (100) Surface; an AES-LEED Study. Surface Science 87 (1): 1-12.

[5] Shelton, J. C.; Patil, H. R.; Blakely, J. M. (1974) Equilibrium segregation of carbon to a nickel (111) surface: A surface phase transition. Surface Science 43 (2): 493-520.

[6] Li, X.; Cai, W.; Colombo, L.; Ruoff, R. S. (2009) Evolution of Graphene Growth on Ni and Cu by Carbon Isotope Labeling. Nanoletters 9 (12): 4268-4272.

556 [7] Yu, Q.; Lian, J.; Siriponglert, S.; Li, H.; Chen, Y. P.; Pei, S.-S. (2008) Graphene segregated on
557 Ni surfaces and transferred to insulators. Applied Physics Letters 93 (11): 113103-3.
558
559 [8] Siegel, D. J.; Hamilton, J. C. (2005) Computational Study of Carbon Segregation and Diffusion
560 within a Nickel Grain Boundary. Acta Macterialia 53 (1): 87-96.
561
562 [9] Kozlov, S. M.; Vines, F.; Goerling, A. (2011) Bonding Mechanisms of Graphene on Metal
563 Surfaces. J. Phys. Chem. C 116 (13): 7360-7366.
564
565 [10] Cepek, C.; Goldoni, A.; Modesti, S. (1996) Chemisorption and Fragmentation of C60 on
566 Pt(111) and Ni(110). Phys. Rev. B 53 (11): 7466-7472.
567
568 [11] Foiles, S. M.; Baskes, M. I.; Daw, M. S. (1986) Embedded-atom-method Functions for the fcc
569 Metals Cu, Ag, Au, Ni, Pd, Pt, and their Alloys. Phys. Rev. B 33 (12): 7983-7991.
570
571 [12] Foiles, S. M. (1985) Calculation of the Surface Segregation of Ni-Cu Alloys with the use of
572 the Embedded-atom Method. Phys. Rev. B 32 (12): 7685-7693.
573
574 [13] Usachov, D.; Dobrotvorskii, A. M.; Varykhalov, A.; Rader, O.; Gudat, W.; Shikin, A. M.;
575 Adamchuk, V. K. (2008) Experimental and theoretical study of the morphology of commensurate
576 and incommensurate graphene layers on Ni single-crystal surfaces. Phys. Rev. B 78 (8): 085403.
577
578 [14] Fedorova, A. V.; Varykhalovb, A. Yu.; Dobrotvorskiia, A. M.; Chikinaa, A. G.; Adamchuka, V.
579 K.; Usachova, D. Yu. (2011) Structure of Graphene on the Ni(110) Surface. Physics of the Solid
580 State 53 (9): 1952-1956.
581
582 [15] Rasuli, R.; Mostafavi, Kh.; Davoodi J. (2014) Molecular dynamics simulation of graphene
583 growth on Ni(100) facet by chemical vapor deposition. J. of Appl. Phys. 115 (2): 024311.
584
585 [16] Ataca, A.; Ciraci, S. (2011) Perpendicular Growth of Carbon Chains on Graphene from First-
586 Principles. Phys. Rev. B 83 (23): 235417.
587
588 [17] Reina, A.; Jia, X.; Ho, J.; Nezich, D.; Son, H.; Bulovic, V.; Dresselhaus, M. S.; Kong, J. (2009)
589 Large Area, Few-Layer Graphene Films on Arbitrary Substrates by Chemical Vapor Deposition.
590 Nanoletters 9 (1): 30-35.
591
592 [18] De Arco, L. G.; Yi, Z.; Kumar, A.; Chongwu, Z. (2009) Synthesis, Transfer, and Devices of
593 Single- and Few-Layer Graphene by Chemical Vapor Deposition. Nanotechnology, IEEE
594 Transactions 8 (2): 135-138.
595
596 [19] Kim, K. S.; Zhao, Y.; Jang, H.; Lee, S. Y.; Kim, J. M.; Kim, K. S.; Ahn, J.-H.; Kim, P.; Choi, J.-
597 Y.; Hong, B. H. (2009) Large-scale pattern growth of graphene films for stretchable transparent
598 electrodes. Nature 457 (7230): 706-710.
599

600   [20] Isett, L. C.; Blakely, J. M. (1975) Binding of carbon atoms at a stepped - Ni surface. Journal
601   of Vacuum Science and Technology 12 (1): 237-241.

602

603   [21] Gamo, Y.; Nagashima, A.; Wakabayashi, M.; Terai, M.; Oshima, C. (1997) Atomic structure
604   of monolayer graphite formed on Ni(111). Surface Science 374 (1-3): 61-64.

605

606   [22] Seung Jin, C.; Fethullah, G.; Scedil; Ki Kang, K.; Eun Sung, K.; Gang Hee, H.; Soo Min, K.;
607   Hyeon-Jin, S.; Seon-Mi, Y.; Jae-Young, C.; Min Ho, P.; Cheol Woong, Y.; Didier, P.; Young Hee,
608   L. (2009) Synthesis of Large-Area Graphene Layers on Poly-Nickel Substrate by Chemical Vapor
609   Deposition: Wrinkle Formation. Advanced Materials 21 (22): 2328-2333.

610

611   [23] Reina, A.; Thiele, S.; Jia, X.; Bhaviripudi, S.; Dresselhaus, M.; Schaefer, J.; Kong, J. (2009)
612   Growth of large-area single- and Bi-layer graphene by controlled carbon precipitation on
613   polycrystalline Ni surfaces. Nano Research 2 (6): 509-516.

614

615   [24] Nair, R. R.; Blake, P.; Grigorenko, A. N.; Novoselov, K. S.; Booth, T. J.; Stauber, T.; Peres,
616   N. M. R.; Geim, A. K. (2008) Fine Structure Constant Defines Visual Transparency of Graphene.
617   Science 320 (5881): 1308.

618

619   [25] Bengaard, H. S.; Nørskov, J. K.; Sehested, J.; Clausen, B. S.; Nielsen, L. P.; Molenbroek, A.
620   M.; Rostrup-Nielsen, J. R. (2002) Steam Reforming and Graphite Formation on Ni Catalysts.
621   Journal of Catalysis 209 (2): 365-384.

622

623   [26] Beebe, T. P.; Goodman, D. W.; Kay, B. D.; Yates, J. T. (1987) Kinetics of the activated
624   dissociative adsorption of methane on the low index planes of nickel single crystal surfaces. The
625   Journal of Chemical Physics 87 (4): 2305-2315.

626

627   [27] Lander, J. J. ; Kern, H. E.; Beach, A. L. (1952) Solubility and Diffusion Coefficient of Carbon
628   in Nickel: Reaction Rates of NickelCarbon Alloys with Barium Oxide. Journal of Applied Physics
629   23 (12): 1305 -1309.

630

631   [28] Novoselov, K. S.; Geim, A. K.; Morozov, S. V.; Jiang, D.; Zhang, Y.; Dubonos, S. V.;
632   Grigorieva, I. V.; Firsov, A. A. (2004) Electric Field Effect in Atomically Thin Carbon Films. Science
633   306 (5696): 666-669.

634

635   [29] Herbig, M.; Raabe, D.; Li, Y. J.; Choi, P.; Zaefferer, S,; Goto, S. (2014) Atomic-Scale
636   Quantification of Grain Boundary Segregation in Nanocrystalline Material. Phys. Rev. Lett. 112
637   (12): 126103.

638

639   [30] Zangwill, A.; Vvedensky, D. D. (2011) Novel Growth Mechanism of Epitaxial Graphene on
640   Metals. Nanoletters 11 (5): 2092-2095.

641

642   [31] Ozcelik, V. O.; Cahangirov, S.; Ciraci, S. (2012) Epitaxial Growth Mechanisms of Graphene
643   and Effects of Substrates. Phys. Rev. B 85 (23): 235456.

644

645 [32] Li, X.; Cai, W.; An, J.; Kim, S.; Nah, J.; Yang, D.; Piner, R.; Velamakanni, A.; Jung, I.; Tutuc,
646 E.; Banerjee, S. K.; Colombo, L.; Ruoff, R. S. (2009) Large-Area Synthesis of High-Quality and
647 Uniform Graphene Films on Copper Foils. Science 324 (5932): 1312-1314.

648

649 [33] Bae, S.; Kim, H.; Lee, Y.; Xu, X.; Park, J.-S.; Zheng, Y.; Balakrishnan, J.; Lei, T.; Ri Kim, H.;
650 Song, Y. I.; Kim, Y.-J.; Kim, K. S.; Ozyilmaz, B.; Ahn, J.-H.; Hong, B. H.; Iijima, S. (2010) Roll-to-
651 roll production of 30-inch graphene films for transparent electrodes. Nature Nanotechnology 5 (8):
652 574–578.

653

654 [34] Bhaviripudi, S; Jia, X; Dresselhaus, M. S.; Kong, J. (2010) Role of Kinetic Factors in Chemical
655 Vapor Deposition Synthesis of Uniform Large Area Graphene Using Copper Catalyst. Nanoletters
656 10 (10): 4128–4133.

657

658 [35] Lahiri, J.; Lin, Y.; Bozkurt, P.; Oleynik, I. I.; Batzill, M. (2010) An extended defect in graphene
659 as a metallic wire. Nature Nanotechnology 5 (5): 326.

660

661 [36] Li, X.; Zhu, Y.; Cai, W.; Borysiak, M.; Han, B.; Chen, D.; Piner, R. D.; Colombo, L.; Ruoff, R.
662 S. (2009) Transfer of Large-Area Graphene Films for High-Performance Transparent Conductive
663 Electrodes. Nanoletters 9 (12): 4359-4363.

664

665 [37] Landau, L. D.; Lifshitz, E. M. (1986) Theory of Elasticity - Third Edition. Pergamon Press.

666

667 [38] Chen, H.; Zhu, W.; Zhang, Z. (2010) Contrasting Behavior of Carbon Nucleation in the Initial
668 Stages of Graphene Epitaxial growth on Stepped Metal Surfaces. Phys. Rev. Lett. 104 (18):
669 186101.

670

671 [39] Weatherup, R. S.; Bayer , B. C.; Blume , R.; Ducati, C.; Baehtz , C.; Schlögl , R.; Hofmann,
672 S. (2011) In Situ Characterization of Alloy Catalysts for Low-Temperature Graphene Growth.
673 Nanoletters 11 (10): 4154–4160.

674

675 [40] McQuarrie, D. A. (1976) Statistical Mechanics - First Edition. Harper and Row.

676

677 [41] Wise, H.; Oudar, J. (2001) Materials Concepts in Surface Reactivity and Catalysis. Dover
678 Publications, NY.

679

680 [42] Gonis, A.; Meike, A.; Turchi, P. E.A. (1996) Properties of Complex Inorganic Solids; Plenum,
681 New York, US.

682

683 [43] Murata, Y.; Petrova, V.; Kappes, B. B.; Ebnonnasir, A.; Petrov, I.; Xie, Y.-H. ; Ciobanu, C. V.;
684 Kodambaka, S. (2010) Moiré Superstructures of Graphene on Faceted Nickel Islands. ACS Nano
685 4 (11): 6509-6514.

686

687 [44] Papagno, L.; Caputi, L. S. (1984) Determination of graphitic carbon structure adsorbed on
688 Ni(110) by surface extended energy-loss fine-structure analysis. Phys. Rev. B 29: 1483.

690 [45] Wiltner, A; Linsmeier, Ch.; Jacob, T. (2008) Carbon reaction and diffusion on Ni(111),
691 Ni(100), and Fe(110): Kinetic parameters from x-ray photoelectron spectroscopy and density
692 functional theory analysis. J. Chem. Phys. 129 (8): 084704.

694 [46] Muñoz, R.; Gómez-Aleixandre, C. (2013) Review of CVD Synthesis of Graphene. Chem.
695 Vap. Deposition 19: 297-322.

697 [47] Zhang, Y.; Zhang, L.; Zhou, C. (2013) Review of Chemical Vapor Deposition of Graphene
698 and Related Applications. Acc. Chem. Res. 46 (10): 2329-2339.

700 [48] Wang, Y.; Zheng, Y.; Xu, X.; Dubuisson, E.; Bao, Q.; Lu, J.; Loh, K. P. (2011) Electrochemical
701 Delamination of CVD-Grown Graphene Film: Toward the Recyclable Use of Copper Catalyst.
702 ACS Nano 5 (12): 9927-9933.

704 [49] Gao, L.; Ren, W.; Xu, H.; Jin, L.; Wang, Z.; Ma, T.; Ma, L.-P.; Zhang, Z.; Fu, Q.; Peng, L.-M.;
705 Bao, X.; Cheng, H.-M. (2012) Repeated growth and bubbling transfer of graphene with millimetre-
706 size single-crystal grains using platinum. Nat. Commun. 3: 1.

708 [50] Mafra, D. L.; Ming, T.; Kong. J. (2015) Facile graphene transfer directly to target substrates
709 with a reusable metal catalyst. Nanoscale 7: 14807.

711 [51] Dahal, A.; Batzill, M. (2014) Graphene–nickel interfaces: a review. Nanoscale 6: 2548.

713 [52] Xu, Z.; Yan, T.; Liu, G.; Qiao, G.; Ding, F. (2016) Large scale atomistic simulation of single-
714 layer graphene growth on Ni(111) surface: molecular dynamics simulation based on a new
715 generation of carbon–metal potential. Nanoscale 8: 921.

717 [53] Delamoreanu, A.; Rabot, C.; Vallee, C.; Zenasni, A. (2014) Wafer scale catalytic growth of
718 graphene on nickel by solid carbon source. Carbon 66: 48.

720 [54] Wu, T.; Zhang, X.; Yuan, Q.; Xue, J.; Lu, G.; Liu, Z.; Wang, H.; Wang, H.; Ding, F.; Yu, Q.;
721 Xie, X.; Jiang, M. (2016) Fast growth of inch-sized single-crystalline graphene from a controlled
722 single nucleus on Cu–Ni alloys. Nat. Mater. 15: 43.

724 [55] Garlow, J. A.; Barrett, L. K.; Wu, L.; Kisslinger, K.; Zhu, Y.; Pulecio, J. F. (2016) Mechanisms
725 of graphene growth by chemical vapour deposition on transition metals. Sci. Rep. 6: 19804.

727 [56] Seah, C-M.; Vigolo, B.; Chai, S-P.; Ichikawa, S.; Gleize, J.; Le Normand, F.; Aweke, F.;
728 Mohamed, A. R. (2016) Sequential synthesis of free-standing high quality bilayer graphene from
729 recycled nickel foil. Carbon 96: 268.

731 [57] Ren, Z.; Meng, N.; Shehzad, K.; Xu, Y.; Qu, S.; Yu, B.; Luo, J. K. (2015) Mechanical
732 properties of nickel-graphene composites synthesized by electrochemical deposition.
733 Nanotechnology 26: 065706.

735 [58] Hohenberg, P.; Kohn, W. (1964) Inhomogeneous Electron Gas. Phys. Rev. 136:B864–B871.

737 [59] Giannozzi, P.; Baroni, S.; Bonini, N.; Calandra, M.; Car, R.; Cavazzoni, C.; Ceresoli, D.;
738 Chiarotti, G. L.; Cococcioni, M.; Dabo, I.; Dal Corso, A.; Fabris, S.; Fratesi, G.; de Gironcoli, S.;
739 Gebauer, R.; Gerstmann, U.; Gougoussis, C.; Kokalj, A.; Lazzeri, M.; Martin-Samos, L.; Marzari,
740 N.; Mauri, F.; Mazzarello, R.; Paolini, S.; Pasquarello, A.; Paulatto, L.; Sbraccia, C.; Scandolo, S.;
741 Sclauzero, G.; Seitsonen, A. P.; Smogunov, A.; Umari, P.; Wentzcovitch, R. M. (2009) QUANTUM
742 ESPRESSO: a modular and open-source software project for quantum simulations of materials.
743 J. Phys.:Condens. Matter 21: 395502.

745 [60] Perdew, J. P.; Burke, K.; Ernzerhof, M. (1996) Generalized Gradient Approximation Made
746 Simple. Phys. Rev. Lett. 77:3865–3868.

748 [61] Dal Corso, A. (2014) Pseudopotentials periodic table: From H to Pu. Comput. Mater. Sci. 95:
749 337-350.

751 [62] Grimme, S.; (2006) Semiempirical GGA-type density functional constructed with a long-range
752 dispersion correction. J. Comp. Chem. 27: 1787.

754 [63] Kittel, C. (2005) Introduction to Solid State Physics, 8th edition. John Wiley and Sons, NJ.

756 [64] Lee,B-J.; Shim, J-H.; Baskes, M. I. (2003) Semiempirical atomic potentials for the fcc metals
757 Cu, Ag, Au, Ni, Pd, Pt, Al, and Pb based on first and second nearest-neighbor modified embedded
758 atom method. Phys. Rev. B 68: 144112.

760 [65] Chung, Y. W. (2001) Practical Guide to Surface Science and Spectroscopy. Academic Press,
761 CA.

763 [66] Bianchini, F.; Patera, L. L.; Peressi, M.; Africh, C.; Comelli, G. (2014) Atomic Scale
764 Identification of Coexisting Graphene Structures on Ni(111). J. Phys. Chem. Lett. 5 (3): 467-473.

766 [67] Zhao, W.; Kozlov, S. M.; Höfert, O.; Gotterbarm, K.; Lorenz, M. P. A.; Viñes, F.; Papp, C.;
767 Göling, A.; Steinrück, H-P. (2011) Graphene on Ni(111): Coexistence of Different Surface
768 Structures. J. Phys. Chem. Lett. 2 (7): 759-764.

770 [68] Wang, Y.; Barcaro, G.; Negreiros, F. R.; Visart de Bocarmé, T.; Moors, M.; Kruse, N.; Hou,
771 M.; Fortunelli, A. (2013) Adsorption-Induced Restructuring and Early Stages of Carbon-Nanotube
772 Growth on Ni Nanoparticles. Chem. Eur. J. 19: 406-413.
773

774 [69] Mueller J. E.; van Duin A. C. T. ; Goddard III W. A. (2010) Development and Validation of
775 ReaxFF Reactive Force Field for Hydrocarbon Chemistry Catalyzed by Nickel. J. Phys. Chem. C
776 114: 4939–4949.

778 [70] See Supplemental Material at [URL will be inserted by publisher] for additional information
779 and results from the theoretical calculations performed in this work.

781 [71] Patera, L. L.; Bianchini, F.; Africh, C.; Dri, C.; Soldano, G.; Mariscal, M. M.; Peressi, M.;
782 Comelli, G. (2018) Real-time imaging of adatom-promoted graphene growth on nickel. Science
783 359: 1243-1246.

785 [72] Zou, Z.; Carnevali, V.; Jugovac, M.; Patera, L. L.; Sala, A.; Panighel, M.; Cepek, C.; Soldano,
786 G.; Mariscal, M. M.; Peressi, M.; Comelli, G.; Africh, C. (2018) Graphene on nickel (100)
787 micrograins: Modulating the interface interaction by extended moiré superstructures. Carbon 130:
788 441-447.